ChemComm

Cation Coordination Polyhedra Lead to Multiple Lengthscale Organization in Aqueous Electrolytes

Journal:	*ChemComm*
Manuscript ID	CC-COM-05-2023-002416.R1
Article Type:	Communication

Journal Name

ARTICLE TYPE

Cite this: DOI: 00.0000/xxxxxxxxxx

Cation Coordination Polyhedra Lead to Multiple Length-scale Organization in Aqueous Electrolytes†

Yihui Wei,*[a] Emily T. Nienhuis,**[b‡] Sebastian T. Mergelsberg,[b‡] Trent R. Graham,[b‡] Qing Guo,[a] Gregory K. Schenter,[b‡] Carolyn I. Pearce[b‡] and Aurora E. Clark***[a]

Received Date
Accepted Date

DOI: 00.0000/xxxxxxxxxx

Understanding multiple lengthscale correlations in the pair distribution functions (PDFs) of aq. electrolytes is a persistent challenge. Here, the coordination chemistry of polyoxoanions supports an ion-network of cation-coordination polyhedra in $NaNO_{3(aq)}$ and $NaNO_{2(aq)}$ that induce long-range solution structure. Oxygen correlations associated with Na^+-coordination polyhedra have two characteristics lengthscales; 3.5 - 5.5 Å and 5.5 - 7.5 Å the latter solely associated oligomers. The PDF contraction between 5.5 - 7.5 Å observed in many electrolytes is attributed to the distinct O$\cdots$O correlation found in dimers and dimer subunits within oligomers.

Highly concentrated solutions are gaining importance due to aq. battery technologies[1–4] and industrial waste processing.[5] Solution organization influences transport and phase behavior and is measured using total PDFs, labelled $G(r)$, obtained from X-ray or neutron total scattering. Much work has focused upon identifying ion-solvation, contact ion pairs (CIPs) and solvent separated ion pairs (SSIPs), and specific ion effects. Approaching electrolyte saturation there is insufficient H_2O to form complete ion solvation shells, increasing CIPs and SSIPs and inducing pair correlations in the PDF at two characteristic distances: 3.5 - 5.5 Å (the **mid-range**, 2^{nd} nearest neighbors) and 5.5 - 7.5 Å (the **long-range**, the 3^{rd} - 4^{th} neighbors). Overlapping atom-pair correlations complicate interpretation of the mid-range PDF,[6,7] which is exacerbated at long-range and as concentration increases. Mid-range water O-atom $O_W\cdots O_W$ correlations occur between 3.5 - 5.5 Å (centered at 4.5 Å)[8] but overlap with ion$\cdots$O distances for many halides (2.8 - 3.6 Å) and polyoxoanions (3.7 Å for NO_2^- or NO_3^- and 4.3 Å for SO_4^-). Depending on the ion identities, the mid-range peak may decrease in intensity with increasing concentration (loss of $O_W\cdots O_W$ pairs), change its location or shape as $O_W\cdots$ion correlations increase their prevalence.

Trends in the long-range PDF with electrolyte concentration are similar to pressure-dependent water.[9] Compression from 1 $\longrightarrow$ 3000 bar contracts the $O_W\cdots O_W$ peak from 4.5 to $\sim$ 4.3 Å and decreases its intensity,[10] while the long-range peak contracts and the region in between the mid- and long-range increases intensity. Structural models propose a collapse of the H_2O 2^{nd} shell that causes higher occupancy in the interstitial space with the 3^{rd} shell concomitant with an increase in the water density and potential orientational disorder.[9,11,12] Concentration dependent PDFs of $NaCl_{(aq)}$ exhibit similar trends; the mid-range $O_W\cdots O_W$ slightly *increases* and the contraction at long-range is more pronounced. Originally attributed to similar origins, recent work indicates that the PDF changes derive from the H_2O that reside in the 1^{st} solvation shell of Na^+ *and* Cl^- rather than shifting H_2O between 2^{nd} - 3^{rd} shells.[10] Concentration dependent long-range PDF changes are more ubiquitous, less ion-dependent,[13,14] and are predominantly interpreted via atom-pair types. Study of concentrated $NaOH_{(aq)}$[15,16] indicates highly fluxional extended ion-networks, where coordination to Na^+ and OH^- strongly influence the PDF. We hypothesize that such features may be stabilized by polyoxo anions whose cation binding modes induce clear geometric arrangements. Toward this end, the structure of $NaNO_{2(aq)}$ and $NaNO_{3(aq)}$ at 1, 2.5, 4, 6, 8, 10 molal and saturation were studied through X-ray total scattering at the Advanced Photon Source, beamline 11-ID-B. Classical molecular dynamics (CMD) simulations provide atom-pair and molecular interpretation of simulated X-ray $G(r)$ and contributions from specific atom pairs or groups of partitioned atoms, labelled G^*(r) (see Supplementary Information for details).

Mid-range $G(r)$ features in $NaNO_{2(aq)}$ shown in Figure 1 are reproduced in the CMD, ($NaNO_{3(aq)}$ data in Figure S3), and are correlated with predicted changes to ion speciation. Feature **A** at $\sim$ 1.25 Å represents the intramolecular oxyanion N-O bond. Feature **B** occurs at $\sim$ 2.23 Å in $NaNO_3$ and 2.23 - 2.39 Å in $NaNO_2$ dependant on concentration. At 1 m $NaNO_2$, **B** is centered at 2.48 Å and 1 m $NaNO_3$ at 2.40 Å. **B** broadens and shifts

[a] *Department of Chemistry, University of Utah, Salt Lake City, UT, USA*
[b] *Pacific Northwest National Laboratory, Richland, WA, USA*
* Email: yihui.wei@utah.edu
** Email: emily.nienhuis@pnnl.gov
*** Email: aurora.clark@utah.edu

† Electronic Supplementary Information (ESI) available: [details of any supplementary information available should be included here]. See DOI: 00.0000/00000000.

Table 1 Atom pair correlations that contribute to features **B** - **E** in the simulated PDFs.

$NaNO_{3(aq)}$							
Feature ⟶		**B**		**C - D**		**E**	
Atom Pair ⟶	$O_N\cdots O_N$	$Na\cdots O_W$	$Na\cdots O_N$	$O_W\cdots O_W$	$O_W\cdots O_N$	$O_W\cdots O_W$	$O_W\cdots O_N$
Peak Center (Å) ⟶	2.18	2.25	2.48	2.78, 3.15	2.92	4.5	4.68
$NaNO_{2(aq)}$							
Feature ⟶		**B**		**C - D**		**E**	
Atom Pair ⟶	$O_N\cdots O_N$	$Na\cdots O_W$	$Na\cdots O_N$	$O_W\cdots O_W$	$O_W\cdots O_N$	$O_W\cdots O_W$	$O_W\cdots O_N$
Peak Center (Å) ⟶	2.08	2.26	2.38	2.78, 3.15	2.81	4.56	4.58

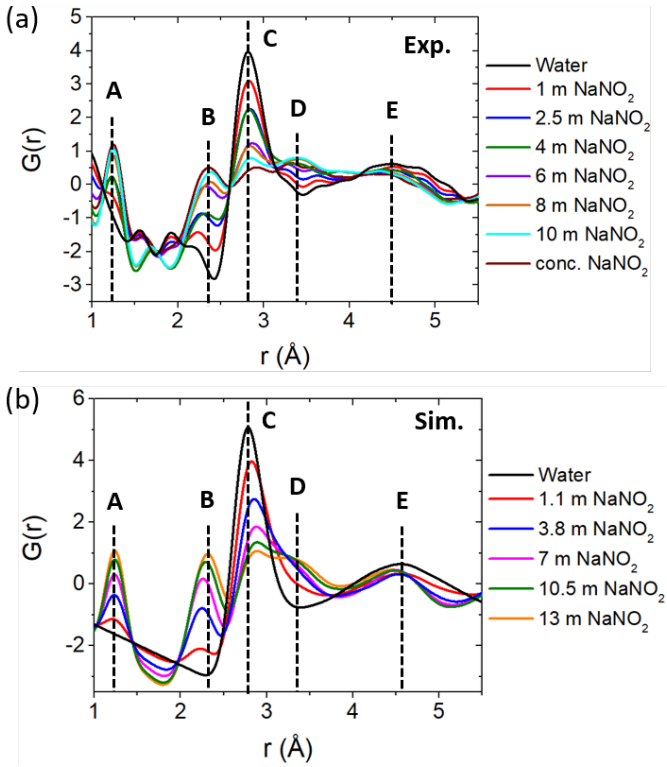

Fig. 1 Short- and mid-range experimental (a) and simulated (b) total X-ray PDFs for $NaNO_{2(aq)}$. Data for $NaNO_{3(aq)}$ are shown in Fig. S3.

to longer distances with increased [$NaNO_x$]; at saturation, **B** has broadened by 0.13 Å and shifted by 0.16 Å for $NaNO_{2(aq)}$, and in $NaNO_{3(aq)}$ it has broadened by 0.07 Å. As observed in Table 1, $Na\cdots O$ and $O_N\cdots O_N$ correlations in the simulated PDF align with **B** (Figure S4). In the case of $NaNO_{3(aq)}$, there is significant overlap in the $O_N\cdots O_N$ and $Na\cdots O_W$ correlations (at 2.18 Å and 2.25 Å, respectively) both of which gain intensity with increasing [$NaNO_3$]. In contrast, the overlap in the $O_N\cdots O_N$ (2.08 Å) and $Na\cdots O_W$ (2.26 Å) is smaller in $NaNO_{2(aq)}$ and more significant overlap occurs between $Na\cdots O_W$ and $Na\cdots O_N$ (centered at 2.38 Å). These data are consistent with trends in Na^+ local coordination, including growth of anion binding (Figure 3a, Table S5) and changes to coordination modes, described using the nomenclature of Ref. 17 (Figure S5) and provided in Table S6. At 1m ∼ 50% and 72 % of Na^+ in the nitrite and nitrate solutions, respectively, are solely hydrated. Yet there is a steady growth of anion binding such all Na^+ are bound to an anion at saturation. Observed CMD denticity of anion coordination was compared to ab initio simulations to ensure realistic behavior (Figure S6). At low electrolyte concentration in the CMD simulations, bi- and monodentate coordination in $NaNO_2$ is observed while monodentate coordination is observed in $NaNO_3$. With increasing electrolyte concentration bidentate coordination increases and ion-pairing is enhanced, leading to di- and tri-nitrate species (Tables S5 - S6). These two phenomena underpin the increased contributions of the $O_N\cdots O_N$ and $Na\cdots O_N$ to **B**.

Feature **C** in Figure 1 is centered at 2.82 Å at 1 m $NaNO_{3(aq)}$ and $NaNO_{2(aq)}$. **C** decreases in intensity and moves to longer distance by 0.1 Å with increasing electrolyte while neighboring feature **D** increases intensity at ca. 3.17 Å for $NaNO_{3(aq)}$ and 3.21 Å for $NaNO_{2(aq)}$. As shown in Figure S7, $O_W\cdots O_W$ contributions at 2.78 - 2.82 Å to **C** decrease as concentration increases. The two electrolytes exhibit anion dependent $O_W\cdots O_N$ distances, occurring at 2.92 Å in $NaNO_{3(aq)}$ and 0.1 Å shorter in $NaNO_{2(aq)}$, consistent with prior DFT studies and increased viscosity for aq. nitrite.[18,19] Feature **D** appears as a shoulder to **C** in the $G(r)$ and is attributed to a new $O_W\cdots O_W$ correlation at 3.15 Å whose origin is not apparent. At 1 m, feature **E** is broad and begins at ∼ 3.48 Å extending to 5.73 Å and centered at ∼ 4.53 Å The contributions to **E** are $O_W\cdots O_W$ (∼ 4.5 Å) and $O_W\cdots O_N$ (4.68 Å and 4.58 Å for $NaNO_{3(aq)}$ and $NaNO_{2(aq)}$, respectively) as shown in Figure S8. With increasing [$NaNO_x$], **D** obscures the start of **E** and there is considerable overlap at 4 Å. The range of **E** contracts by ∼ 0.4 Å in concentrated $NaNO_{3(aq)}$ and is more pronounced in $NaNO_{2(aq)}$. Although there is no distinct shift in the peak maximum for $NaNO_{3(aq)}$, in $NaNO_{2(aq)}$ it shifts from ∼ 4.53 Å in the 1 m solution to 4.40 Å at saturation. In the simulated $G(r)$ the range of the $O_W\cdots O_W$ contribution narrows and the $O_W\cdots O_N$ increases with concentration (recall $O_W\cdots O_N$ is shorter in $NaNO_{2(aq)}$ relative to $NaNO_{3(aq)}$). Like **D**, an interpretation of **E** based upon local coordination to Na^+ is unclear.

The interplay of **C** - **E** indicate *molecular-scale* organization that may influence the long-range. At 1 m, feature **G** occurs at ∼ 6.84 Å (Figure 2), yet as [$NaNO_x$] increases **G** decreases and there is a distinct shift to yield **F**, centered at 6.15 and 6.23 Å in $NaNO_{3(aq)}$ and $NaNO_{2(aq)}$. Here, the $O_W\cdots O_W$ and $O_W\cdots O_N$ are contributors (Figure S10) and prior study of $NaNO_{3(aq)}$ has surmised the replacement of $O_W\cdots O_W$ by $O_W\cdots O_N$.[20] Instead, we hypothesize and test a partition of the atom-pair correlations into two

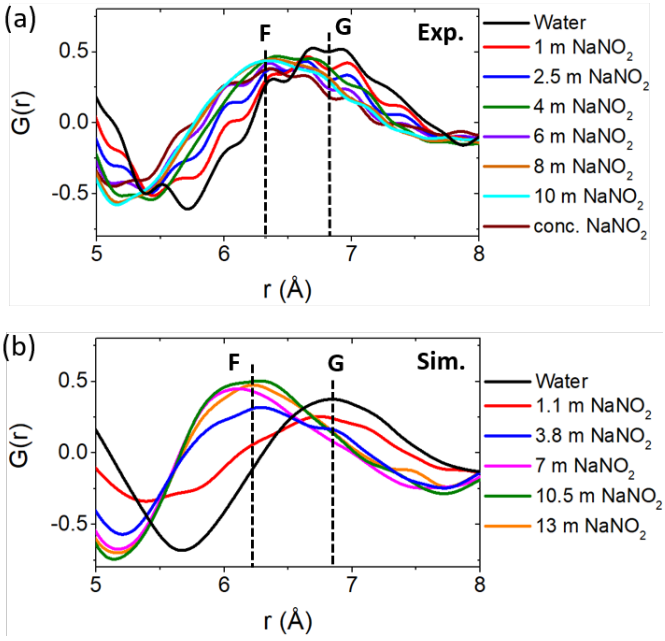

Fig. 2 Long-range experimental (a) and simulated (b) total X-ray PDFs of $NaNO_{2(aq)}$. Data for $NaNO_{3(aq)}$ are shown in Fig. S9.

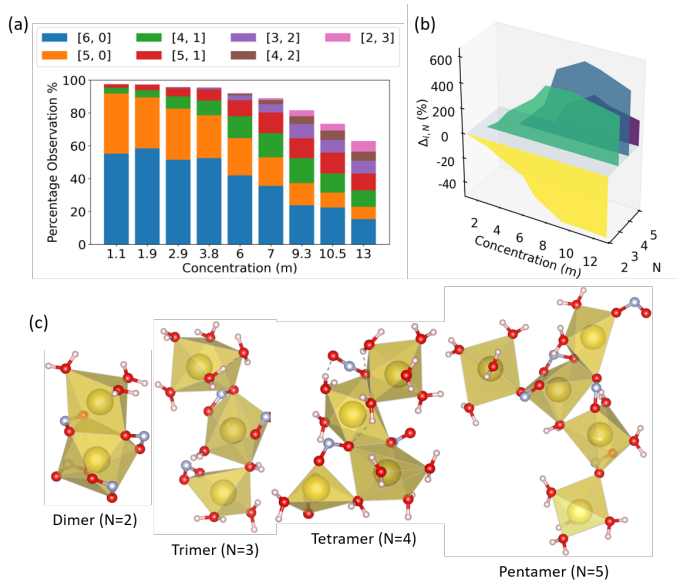

Fig. 3 (a) Top 6 observed coordination environments of Na^+ as a function of [$NaNO_2$] in CMD. Labels [a, b] indicates coordinated H_2O and NO_2^-, respectively (Table S7). (b) The % change $\Delta_{i,N}$ of polyhedron and oligomers of size N as a function of [$NaNO_2$] calculated from CMD. $\Delta_{i,N} = (P_{i,N} - P_{c,N})/P_{c,N}$, where P is the probability at a concentration i relative to the lowest concentration c for which N-oligomer is observed. The decreased observation of N = 3 - 5 at high [$NaNO_2$] is due to low observation highly fluxional large N and are not reported (Table S8). (c) Representative oligomers in $NaNO_{2(aq)}$. This information for $NaNO_3$ is shown in Figure S13.

groups that contribute to $G(r)$ (Figure S11): 1) the ensemble distribution of O_W and O_N that coordinate Na^+; 2) the remaining H_2O outside of Na^+ coordination, referred to as "bulk O" in the remaining discussion. We use a cation-centric partitioning, as anion solvating $O_W \cdots O_W$ were found to have the same RDFs as all other H_2O. This partitioning allows us to test two potential structural origins of the observed long-range shift. First, is that the long-range contraction is an emergent behavior of subtle variations in H_2O intermolecular interactions that do not solvate Na^+. As observed in Figure S12 and Table S7, variations in HB distance of 0.1 Å and 10 ° easily shift in $O_W \cdots O_W$ distances by 0.3 Å at mid-range and extension to the 4 - 5 HB pathways at long-range could lead to the **G** $\longrightarrow$ **F** shift. A second origin may be that the bulk water is replaced by Na^+ coordination complexes, where new $O_W \cdots O_W$ correlations emerge when multiple H_2O solvate the same Na^+, are constrained in between Na^+ as part of SSIPs, and form new $O_W \cdots O_N$ correlations when an H_2O and NO_3^- or NO_2^- coordinate to the same Na^+. Connected coordination polyhedra of Na^+ (oligomers) will have different distances of $O_W \cdots O_W$ and $O_W \cdots O_N$ correlations. The 2^{nd} case is a "molecular" building block perspective of an extended ion-network, and the partitioned contributions to $G(r)$ are referred to as "network O".

With increasing concentration, the composition of Na^+ coordination environments becomes more complex. As shown in Figure 3a there is a systematic increase of coordinating anions; bidentate κ^2 anion coordination 17 to 2 Na^+ is observed in $\sim$ 5% concentrations even at 1 m electrolyte (Table S6). Growth of tridentate μ_2-κ^2:κ^1 anion coordination occurs at 6 m [$NaNO_{3(aq)}$] and 10.4 m [$NaNO_{2(aq)}$]. As saturation is reached, a breadth of tetra to heptadentate anion coordination exists. Concomitantly there is a huge increase of anions coordinating multiple Na^+ to form oligomers. Figure 3b-c presents the oligomer distributions (Table S8) of coordination polyhedra, with representative structures for $NaNO_{2(aq)}$. Anion bridging and corner-sharing connectivity are the most frequently observed (Table S9, Figure S14). Hexamers occur near saturation and stable oligomers appear to exist in a highly fluxional near-percolated network of ion-interactions. This is indicated in Figure S15, where the oligomer size is plotted vs. time. While most oligomers are stable at a size below 6, these species may come together into large highly dynamic clusters up to size 100 that encompass nearly all ions and rapidly break.

Examining the partial $G^*(r)$ of the partitioned bulk O and network O that contribute to the total PDF reveals that the polyhedral building blocks of ion connectivity have distinct O$\cdots$O correlations. Importantly, this is true for both the mid- and long-range features of the PDF. As shown in Figure 4a, the mid-range $G^*(r)$ $O_W \cdots O_W$ peak of the partitioned bulk water is centered at 2.78 Å. We also examined those O_W that reside in the 2^{nd} solvation shell of the Na^+ coordination polyhedra (or at the interface between the polyhdra and bulk water) and observe these O_W have the same correlation as bulk O_W. In contrast, the $G^*(r)$ of O_W solely within the network of Na^+ coordination has a peak at 3.15 Å for $NaNO_{3(aq)}$ and $NaNO_{2(aq)}$. Thus, the growth of feature **D** and decrease of **C** in Figure 1can now be attributed to $O_W \cdots O_W$ comprised of H_2O bound to Na^+ in the ion network.

Figure 4(b) presents the O$\cdots$O $G^*(r)$ at long-range. The $O_W \cdots O_W$ the peak in $G^*(r)$ of the bulk water is centered between 6.7 - 6.8 Å and is assigned to **G** in Figure 1. The O$\cdots$ O in the network of Na-coordination polyhedra has a peak maximum at 6.25 and 6.15 Å for $NaNO_3$ and $NaNO_2$, aligning with **F**. To directly cor-

relate **F** with oligomer concentration, we plot the distribution of oligomers in Figure S17 and the probability distribution of O...O distance as a function of oligomer size in Figure S18. Interestingly, the characteristic c.a. 6 Å **F** peak is a feature of the dimer, and increases in intensity with oligomer size due to the number of dimer sub-units as the oligomer grows. Thus, we definitively show that the **G** ⟶ **F** in the long range originates from characteristic O_W...O_W, O_W...O_N, and O_N...O_N correlations within dimer sub-motifs of oligomers in an extended ion network.

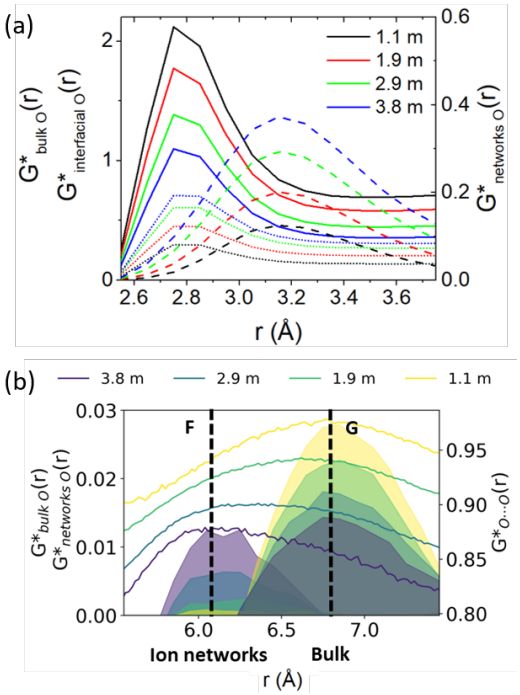

Fig. 4 (a) Mid-range partial XRD PDFs of the two structural models in $NaNO_{2(aq)}$ (Eqn. S4). Solid lines: bulk O ⋯ O; dash lines: networks O ⋯ O; dot lines: interfacial O ⋯ O. (b) Long-range partial XRD PDFs of O⋯O (solid lines) and different oxygen states (shaded lines) in $NaNO_2$ solutions. $G^*(r)$ of bulk O and networks O are aligned by moving the averaged $G^*(r)$ from 5.5-7.5 Å to 0. Data for $NaNO_{3(aq)}$ shown in Figure S16.

Polyoxo anions are shown to facilitate connected cation coordination polyhedra that yield multiscale PDF correlations. Specifically, O_W ⋯ O_W associated with ion solvation, and oligomerization of the coordination polyhedra about a metal cation have two characteristics lengthscales. At the mid-range are O_W correlations within the coordination shell about the same cation, while at the long range O-atom correlations derive from connected coordination complexes, bridged by anions, corner-, edge-, or face-sharing H_2O. The general long-range PDF contraction, observed *ubiquitously* in aq. electrolytes is explained by loss of the many-body bulk water and growth of ion-network O ⋯ O facilitated by well-defined paths along edges of coordination polyhedra.

Y. W.: Methodology, formal analysis, investigation, writing. **E. N.**: Methodology, formal analysis, investigation, writing. S. M.: Methodology. **T. G.**: Visualization. **Q. G.**: Investigation. **G. S.**: Conceptualization, funding acquisition. **C. P.**: Conceptualization, funding acquisition, project administration, supervision. **A.E.C.**: Conceptualization, methodology, funding acquisition, supervision, writing, project administration.

Conflicts of interest

There are no conflicts to declare.

Acknowledgements

This research was supported by Interfacial Dynamics in Radioactive Environments and Materials, an Energy Frontier Research Center (FWP 68932) funded by the U.S. Department of Energy (DOE), Office of Science (SC), Basic Energy Sciences. This research used the Advanced Photon Source, a U.S. DOE SC user facility operated by Argonne National Laboratory under Contract No. DE-AC02-06CH11357. We acknowledge Olaf Borkiewicz and Leighanne Gallington for assistance at 11-ID-B beamline.

Notes and references

1 H. Zhang *et al.*, *Angewandte Chemie International Edition*, 2021, **60**, 598–616.
2 H. Kim *et al.*, *Chemical Reviews*, 2014, **114**, 11788–11827.
3 R.-S. Kuhnel *et al.*, *ACS Energy Letters*, 2017, **2**, 2005–2006.
4 L. Chen *et al.*, *ACS Energy Letters*, 2020, **5**, 968–974.
5 R. A. Peterson *et al.*, *Environmental Science & Technology*, 2018, **52**, 381–396.
6 M. A. Marques *et al.*, *Journal of Physics: Condensed Matter*, 2002, **14**, 7427.
7 M. C. Ribeiro, *J. Phys.: Condensed Matter*, 2005, **17**, 453.
8 K. Amann-Winkel *et al.*, *Chemical Reviews*, 2016, **116**, 7570–7589.
9 R. Leberman and A. Soper, *Nature*, 1995, **378**, 364–366.
10 C. Zhang *et al.*, *Nature Communications*, 2022, **13**, 822.
11 R. Mancinelli *et al.*, *Physical Chemistry Chemical Physics*, 2007, **9**, 2959–2967.
12 G. E. Walrafen, *J. Chem. Phys.*, 1962, **36**, 1035–1042.
13 A. K. Soper and K. Weckström, *Biophys. Chem.*, 2006, **124**, 180–191.
14 P. Gallo *et al.*, *Journal of Molecular Liquids*, 2014, **189**, 52–56.
15 D. Semrouni *et al.*, *Physical Chemistry Chemical Physics*, 2019, **21**, 6828–6838.
16 M. Hellström and J. Behler, *Phys. Chem. Chem. Phys.*, 2017, **19**, 82–96.
17 P. Saxena and N. Thirupathi, *Polyhedron*, 2015, **98**, 238–250.
18 M. Lalitha and L. Senthilkumar, *J. Mol. Graphics and Modelling*, 2014, **54**, 148–163.
19 J. G. Reynolds *et al.*, *Journal of Molecular Liquids*, 2018, **264**, 110–114.
20 T. Megyes *et al.*, *The Journal of Physical Chemistry B*, 2009, **113**, 4054–4064.